

Revisiting short-plateau SN 2018gj

V. P. Utrobin^{1,2*} and N. N. Chugai²

¹*NRC “Kurchatov Institute”, acad. Kurchatov Square 1, Moscow, 123182, Russia.

²Institute of Astronomy, Russian Academy of Sciences, Pyatnitskaya St. 48, Moscow, 119017, Russia.

*Corresponding author(s). E-mail(s): utrobin@itep.ru;
Contributing authors: nchugai@inasan.ru;

Abstract

We present an alternative model of unusual type-IIP SN 2018gj. Despite the short plateau and early gamma-rays escape seeming to favor low-mass ejecta, our hydrodynamic model requires a large ejected mass ($\approx 23 M_{\odot}$). The high ejecta velocity, we find from hydrogen lines in early spectra, is among crucial constraints on the hydrodynamic model. We recover the wind density that rules out a notable contribution of the circumstellar interaction to the bolometric luminosity. The early radioactive gamma-rays escape is found to be due to the high velocity of ^{56}Ni , whereas the asymmetry of the $\text{H}\alpha$ emission is attributed to the asymmetry of the ^{56}Ni ejecta. The available sample of type-IIP supernovae studied hydrodynamically in a uniform way indicates that the asymmetry of the ^{56}Ni ejecta is probably their intrinsic property. Hydrogen lines in the early spectra of SN 2018gj and SN 2020jfo are found to imply a clumpy structure of the outer ejecta. With two already known similar cases of SN 2008in and SN 2012A we speculate that the clumpiness of the outer ejecta is inherent to type-IIP supernovae related to the red supergiant explosion.

Keywords: hydrodynamics – methods: numerical – supernovae: general – supernovae: individual: SN 2018gj

1 Introduction

Type-IIP and -IIL supernovae (SNe IIP/L) compose the dominant category of core-collapse supernovae that originate from progenitors with the main-sequence masses of $9 - 25 M_{\odot}$ (Woolesley et al., 2002). The unbiased sample of 13 SNe IIP explored via the uniform hydrodynamic approach (Utrobin and Chugai, 2024) is roughly consistent with the predicted mass range of SNe IIP/L progenitors, although ejecta masses $\lesssim 12 M_{\odot}$ are somewhat scarce in this sample.

However, the modeling of SN 2020jfo with a short light-curve plateau (~ 60 d) results in the ejecta mass of $\approx 6 M_{\odot}$ (Teja et al., 2022; Utrobin

and Chugai, 2024). Moreover, Hiramatsu et al. (2021) reported on three SNe IIP with short plateaus (SN 2008Y, SN 2006ai, and SN 2016egz) and the inferred hydrogen envelope masses of about 1, 2, and $4 M_{\odot}$, respectively. Hence, the low-mass ejecta — although rare among SNe IIP — are not extremely scarce.

The type-IIP supernova SN 2018gj in the galaxy NGC 6217 discovered by Wiggins (2018) and explored in detail by Teja et al. (2023) is the short-plateau (~ 75 d) object. Another notable feature is a rapid luminosity decline at the radioactive tail just after the plateau stage. At first glance, both the short plateau and the early gamma-ray leakage suggest a low-mass ejecta that

seems to be in line with the hydrodynamic modeling (Teja et al., 2023). However, obvious dissimilarities between SN 2018gj and SN 2020jfo — longer plateau of the former (75 vs 60 d), higher plateau luminosity, H α emission asymmetry, and early gamma-ray leakage — suggest that SN 2018gj is a special case and not just a twin of SN 2020jfo. The above said motivates us to revisit the case of SN 2018gj.

There are two additional important reasons for this. First, the previous hydrodynamic model of SN 2018gj requires $0.1 - 0.2 M_{\odot}$ in the circumstellar (CS) shell to account for the early luminosity peak (Teja et al., 2023). Meanwhile, the issue of the CS matter density can be explored based on available spectra in a way similar to that of SN 2020jfo (Utrobin and Chugai, 2024), though with some correction. For SN 2018gj, the early spectra at 1 – 3 days are absent, so we cannot use the early-time broad He II 4686 Å emission to infer the maximal expansion velocity. However, we can use hydrogen lines at a somewhat later stage and obtain the maximal velocity from the absorption blue edge.

Secondly, the early spectrum of SN 2018gj provides us with the opportunity to verify a possible ubiquity of the clumpy structure of the outer ejecta of SNe IIP. This phenomenon is revealed by SN 2008in (Chugai and Utrobin, 2014) and SN 2012A (Utrobin and Chugai, 2015) via the anomalously low ratio of optical depths H α /H β (~ 1 , instead of a theoretical ratio of 7.25); we dub this paradox the “H α /H β -problem”. The H α /H β -problem is resolved assuming the clumpy outer ejecta (Chugai and Utrobin, 2014). The ejecta clumpiness was attributed to the propagation of the explosion shock wave in the red supergiant (RSG) envelope, perturbed before that by a vigorous convection. The issue of a shock breakout (SBO) in the RSG envelope modified by the convection has recently received attention and has been explored via three-dimensional (3D) simulations (Goldberg et al., 2022b,a).

In Section 2, we recover the maximal expansion velocities via the modeling of hydrogen lines that also reveals the H α /H β -problem. We then find the basic parameters of SN 2018gj via the hydrodynamic modeling of the relevant set of observational data including the maximal ejecta

velocity (Section 3). In Section 4, we infer the density of the presupernova (pre-SN) wind and show that the ejecta interaction with the CS matter cannot affect the light curve. Finally, we discuss the results and some features of the SNe IIP sample studied with a uniform hydrodynamic approach.

Below, we use the distance modulus $\mu = 31.46 \pm 0.15$ ($D = 19.61$ Mpc), the reddening $E(B - V) = 0.08 \pm 0.02$ mag, and the explosion date of JD 2458127.8 (Teja et al., 2023).

2 High-velocity ejecta

2.1 Outermost ejecta velocity

The parameters of SN IIP — ejecta mass, explosion energy, and pre-SN radius — can be reliably inferred from the light curve and expansion velocities via modeling the well-observed SNe based on all sensitive observables. Particular attention should be paid to the maximum ejecta velocity that is associated with the thin boundary dense shell formed during the SBO (Grassberg et al., 1971; Chevalier, 1981). Usually, the hydrodynamic modeling of SNe IIP ignores the ejecta velocities at the early stage ($t < 10$ d) focusing primarily on the photospheric velocities at the plateau stage. However, it is well known that SN parameters inferred from the description of the SN IIP plateau luminosity and the expansion velocities at the plateau stage suffered from parameter degeneracy (Goldberg and Bildsten, 2020). On the other hand, taking into account the outermost ejecta velocity secures the unique choice of principal SN parameters (Utrobin and Chugai, 2019).

Another key role of the maximal ejecta velocity is the constraining of the CS density, which permits us to rule out a dense CS shell frequently invoked to describe the early luminosity peak. Indeed, a high ejecta velocity indicates the absence of significant deceleration and thus excludes a dense CS shell. The case of SN 2020jfo illustrates the efficiency of this observational constraint (Utrobin and Chugai, 2024).

The available set of SN 2018gj spectra (Teja et al., 2023) starts from day 5 after the SN explosion. The hydrogen and helium lines with a shallow broad P Cygni line profile are seen already on day 5, while the H α line becomes pronounced on day 7. We recover the velocity at the photosphere (v_p) and the maximum velocity of the

Table 1 The photospheric and maximal velocities and the Sobolev optical depth in SN 2018gj and SN 2020jfo ejecta on day 7

SN	Line	v_p	v_{max}	τ_p
2018gj	H γ	9.5 ± 0.5	15.2 ± 1	0.23 ± 0.05
	H β	11 ± 0.5	16.5 ± 1	0.27 ± 0.05
	HeI	10 ± 0.5	15.5 ± 1	0.25 ± 0.05
	H α	10 ± 0.5	15 ± 1	0.27 ± 0.05
2020jfo	H γ	9.5 ± 0.5	15.2 ± 1	0.2 ± 0.05
	H β	9.5 ± 0.5	16.15 ± 1	0.4 ± 0.05
	HeI	9 ± 0.5	15.3 ± 1	0.25 ± 0.05
	H α	9 ± 0.5	15.3 ± 1	0.33 ± 0.05

Velocities are measured in 1000 km s^{-1} .

ejecta (v_{max}) for hydrogen and He II 5876 \AA lines using the spectrum on day 7.

The line profile is modeled assuming a spherical atmosphere attached to a photosphere with the sharp boundary. The Sobolev optical depth τ and emissivity η are set parametrically as $\tau = \tau_p(v_p/v)^3$ and $\eta = \eta_p(v_p/v)^q$, where q is in the range of 6 – 9. The radiation transfer is calculated using the Monte Carlo technique. The photon with the weight w scatters at the resonant point v with the probability of $(1 - e^{-\tau})$; the scattered photon acquires the weight λw with the albedo $\lambda = 1$ for H α , while $\lambda < 1$ for H β and H γ due to the transition to lower levels. The net line emission is described as the term ηw added to the weight of scattered photons. The parameter of net emissivity is in the range of $0 < \eta_p < 4$ with the maximum value for H α .

The line photon striking the photosphere can be reflected diffusively, which results in a blueshift compared to the case of absorbing photosphere (Fig. 1b, inset). With the density at the photosphere provided by the hydrodynamic model $\approx 10^{-13} \text{ g cm}^{-3}$ on day 7 and the observational temperature of $\approx 10000 \text{ K}$ (Teja et al., 2023), the free-free absorption is the major absorption mechanism at the photosphere. Using Boltzmann-Saha equations for ionization and excitation, we estimate the absorption probability (ϵ) in the range of 0.002 – 0.007 for wavelengths between H γ and H α . The spherical albedo in the case of the high optical depth and $\epsilon < 0.2$ can be approximated as $A \approx 1 - 2\sqrt{\epsilon}$ (Sobolev, 1975). This results in $A \approx 0.83 - 0.91$ which means that the diffusive reflection must be taken into account.

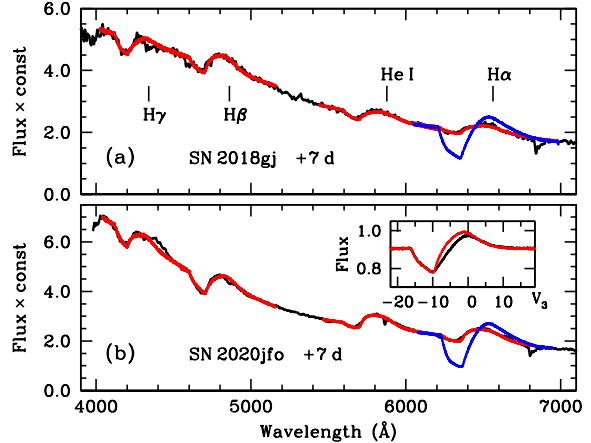


Fig. 1 Spectra of SN 2018gj (Panel (a)) and SN 2020jfo (Panel (b)) on day 7 showing H γ , H β , He I 5876 \AA , and H α lines with the overlaid line models (red line). For the H α line we show a case with the theoretical ratio of the H α /H β optical depths (blue line); this illustrates the “H α /H β problem” related to the clumpiness (see Section 2.2). Inset in the lower panel displays the H β line profile for the photosphere albedo $A = 1$ (red line) and $A = 0$ (black line) that demonstrates the effect of the diffuse reflection from the photosphere.

The recovered velocities and the Sobolev optical depth at the photosphere on day 7 are given in Table 1. The parameters of SN 2020jfo with the shorter plateau are included for comparison. The uncertainties shown in Table 1 are typical scatter of the results that is estimated via parameter variations with a visual model fitting in each case and then rounded. The mean maximal velocity for the considered lines of SN 2018gj is $v_{max} = 15500 \pm 500 \text{ km s}^{-1}$. Surprisingly, the inferred values for both SNe are similar. In the case of SN 2020jfo, we obtained the maximal velocity of 16500 km s^{-1} from the broad He II 4686 \AA emission on day 2.1 (Utrobin and Chugai, 2024). Although the early spectra are lacking for SN 2018gj, the inferred similar maximal velocity on day 7 in both SNe suggests that the maximal velocity on day 2.1 for SN 2018gj could be comparable to that of SN 2020jfo, assuming that the rate of the velocity evolution is the same for both SNe.

2.2 Clumpiness of outer ejecta

A striking feature is a comparable value of the Sobolev optical depth for H α and H β demonstrated by both SNe. This fact is in sharp contradiction with the theoretical ratio $\tau_{23}/\tau_{24} =$

7.25. The $H\alpha/H\beta$ problem is clearly demonstrated in Fig. 1 that shows the unacceptably deep $H\alpha$ absorption expected theoretically based on the $H\beta$ optical depth.

In fact, this phenomenon has been already recognized in type-IIP SN 2008in (Utrobin and Chugai, 2013) and explored in terms of the ejecta clumpy structure (Chugai and Utrobin, 2014). The effect of clumpiness has been found also in SN 2012A (Utrobin and Chugai, 2015). It is reasonable to assume that in SN 2018gj and SN 2020jfo the outer ejecta are composed by dense clumps that are optically thick ($\tau \gg 1$) in hydrogen lines, whereas the rest of the volume is optically thin ($\tau \ll 1$) for the same lines. In that case, the absorbed (scattered) fraction of the photosphere flux at a certain radial velocity is determined by the occultation optical depth, or average volume filling factor (f), at the resonant plane¹ and not by the Sobolev optical depth as expected for the homogeneous density distribution. Remarkably, the clumpy structure of the outer ejecta in SN 2008in, SN 2012A, SN 2018gj, and SN 2020jfo is characterized by the similar filling factor ($f \sim 0.3$), which apparently is the intrinsic property of a mechanism responsible for the clumpiness.

The clumpy structure presumably arises during the explosion shock-wave propagation in the outer layers of the RSG star where a vigorous convective motion with the convective velocity comparable to the sonic speed $v_c \sim c_s$ bring about high-amplitude density perturbations $\Delta\rho/\rho \approx (v_c/c_s)^2 \sim 1$ (Chugai and Utrobin, 2014). These density fluctuations affect the shock-wave propagation, thus producing the clumpiness of the outer ejecta. It goes without saying that the one-dimensional (1D) hydrodynamics of SNe IIP is not able to reproduce the clumpiness of the outer ejecta, however, 3D hydrodynamics hopefully could do so in the future (cf. Goldberg et al., 2022b).

¹For the space filled by bodies with the filling factor f the relative area of body sections in the random plane is also f .

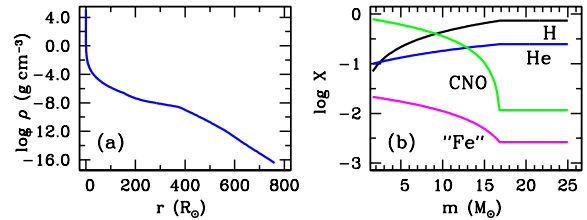


Fig. 2 The structure of the pre-SN model. Panel (a): the density distribution as a function of radius. Panel (b): the chemical composition. Mass fraction of hydrogen (black line), helium (blue line), CNO elements (green line), and Fe-peak elements excluding radioactive ^{56}Ni (magenta line) in the ejected envelope. The central core of $1.6 M_{\odot}$ is omitted.

3 Hydrodynamic model

3.1 Model overview

We use the radiation hydrodynamics code CRAB with the radiation transfer in the gray approximation (Utrobin, 2004, 2007). The pre-SN is the hydrostatic nonevolutionary RSG model. The term “nonevolutionary” means that the pre-SN density distribution and the chemical composition are modified in order to reproduce the light curve and expansion velocities. There are two reasons to use the nonevolutionary model: (i) the explosion of an evolutionary model in a 3D hydrodynamics results in the strong modification of the pre-SN density and composition distributions in the hydrodynamic time scale; (ii) the explosion of the evolutionary RSG star using the 3D hydrodynamics is not able to reproduce the light curve of the standard type-IIP SN 1999em (Utrobin et al., 2017). These arguments compel us to use a nonevolutionary model that should be considered as a palliative tool to compensate for the lack of an adequate “ab initio” model with the appropriate physics included.

The explosion is initiated by a supersonic piston applied to the stellar envelope at the boundary with the $1.6 M_{\odot}$ collapsing core. The description of the light curve and velocities at the photosphere, including the outermost expansion velocity, requires a tuning of the pre-SN density and chemical-composition distributions that should have smooth density and composition gradients at the metals/He and He/H interfaces (Fig. 2). The smoothed gradients presumably reflect mixing in 3D simulations of the SN IIP explosion (Utrobin et al., 2017).

Table 2 Parameters of hydrodynamic model

Parameter	Unit	Value	Error
Ejected mass	M_{\odot}	23.4	± 1.6
Explosion energy	10^{51} erg	1.84	± 0.14
Pre-SN radius	R_{\odot}	775	± 55
^{56}Ni mass	M_{\odot}	0.031	± 0.005

3.2 Results

The hydrodynamic model with parameters listed in Table 2 provides an optimal fit to the bolometric light curve together with the velocity at the photosphere (Fig. 3). The model maximal velocity of 15800 km s^{-1} is also in reasonable agreement with $v_{max} = 15550 \pm 500 \text{ km s}^{-1}$ inferred above from the hydrogen absorption line profiles in the spectrum on day 7. The missing rising part of the light curve hampers the recovery of the explosion moment with accuracy better than 1.5 d. The overall fit of the light curve and the expansion velocities (Fig. 3) agree with the adopted explosion date JD 2458127.8 (Teja et al., 2023).

Despite the fact that the radiation transfer is treated in the gray approximation, the early R -band magnitude is well reproduced by the model (Fig. 4a). As in the previous SNe IIP models, the initial R -band peak has the double structure that was explained in the case of SN 2017gmr (Utrobin et al., 2021). The first peak is related to the SBO, whereas the second is the outcome of the thin-shell formation. However, it is not clear whether this double-peak structure would remain in 3D hydrodynamics, since density perturbations in the RSG envelope modify the luminosity peak following the SBO (Goldberg et al., 2022b).

The total density and the ^{56}Ni density in the freely expanding ejecta on day 50 are shown in Fig. 4b. The remarkable result of the SN 2018gj modeling is the high velocity of the ^{56}Ni ejecta ($\approx 5280 \text{ km s}^{-1}$) that is imposed by the rapid luminosity decline at the radioactive tail (Fig. 3a). This behavior of the light curve also suggests the total ^{56}Ni mass of $0.031 M_{\odot}$, somewhat larger than the previous estimate of $0.026 M_{\odot}$ (Teja et al., 2023). The inferred ^{56}Ni velocity is significantly larger compared to another short-plateau SN 2020jfo, where the ^{56}Ni ejecta is located in the center with the maximum velocity of 1600 km s^{-1} (Utrobin and Chugai, 2024). The $\text{H}\alpha$ emission

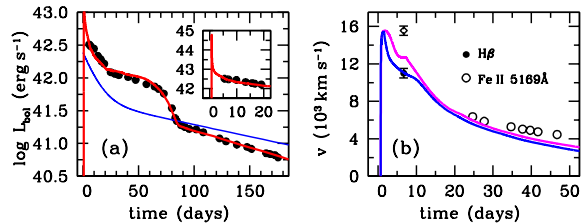


Fig. 3 The bolometric light curve and the evolution of photospheric velocity. Panel (a): the model light curve (red line) overlaid on the bolometric data (circles) (Teja et al., 2023). The blue line is the total power of radioactive ^{56}Ni decay. Inset shows zoom-in of the initial 20 days. Panel (b): the evolution of model velocity defined by the level $\tau_{eff} = 2/3$ (blue line) and $\tau_{\text{Thomson}} = 1$ (magenta line) is compared with the photospheric velocities estimated from the absorption minimum of Fe II 5169 Å (Teja et al., 2023) along with our estimate from the H β line. The outermost ejecta velocity is recovered from the blue absorption wing of hydrogen lines (diamond).

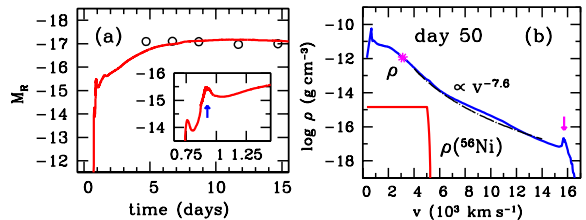


Fig. 4 Panel (a): Rising part of the model light curve in the r -band overplotted on the observational data taken by Teja et al. (2023). Inset shows the fine structure of the narrow peak related to shock breakout. The second fine-structure peak indicated by blue arrow corresponds to the formation of the thin boundary shell marked by an arrow on the right panel. Panel (b): The density and ^{56}Ni distributions vs. velocity in the ejecta on day 50; magenta star indicates the photosphere location, while the magenta arrow shows the boundary thin shell. The dash-dotted line is the power law $\rho \propto v^{-7.6}$.

blueshift (Teja et al., 2023) is likely an effect of the bipolar ^{56}Ni ejecta, whereas the 1D hydrodynamical model treats the ^{56}Ni ejecta as spherically symmetrical. The inferred ^{56}Ni velocity therefore should be considered as the maximal velocity of the asymmetric ^{56}Ni distribution.

The uncertainty in the derived SN parameters can be estimated by a variation of the model parameters around the optimal model. The uncertainties of the distance and the reddening (see Section 1) imply the 15 per cent uncertainty in the bolometric luminosity. The scatter in the plot of the photospheric velocity versus time (Fig. 3b) suggests an uncertainty of 6 per cent in the photospheric velocity. Following Teja et al. (2023), we

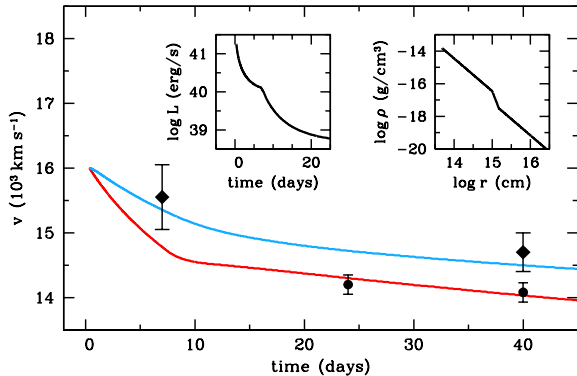


Fig. 5 The CDS velocity (*red line*) and the boundary velocity of the unshocked ejecta (*blue line*) in the model of the SN/wind interaction overlaid on the observed velocities of the CDS (*circles*) and the unshocked ejecta (*diamonds*). The left inset shows the combined luminosity of the forward and reverse shocks; the right inset shows the wind density.

adopt the uncertainty of the plateau length as 2 d, i.e., 2.7 per cent of the plateau duration. With these uncertainties of observables, we find errors of $\pm 55 R_{\odot}$ for the initial radius, $\pm 1.6 M_{\odot}$ for the ejecta mass, $\pm 0.14 \times 10^{51}$ erg for the explosion energy, and $\pm 0.005 M_{\odot}$ for the total ^{56}Ni mass (Table 2).

4 Presupernova wind

The density and radial distribution of the CS matter can be recovered from the CS interaction effects imprinted in spectra of SN 2018gj (Teja et al., 2023). The hydrodynamics of the ejecta interaction with the CS gas is considered in the thin-shell approximation (Chevalier, 1982; Chugai, 2018). The major observables that constrain the CS density distribution are the maximal velocity of the unshocked ejecta inferred from four lines on day 7, the $\text{H}\alpha$ line on day 40, and also the high-velocity narrow absorption (HVNA) in the blue $\text{H}\alpha$ wing on days 24 and 40 that indicate the velocity of the cold dense shell (CDS) (Chugai et al., 2007). The density distribution in the ejecta is approximated by the expression $\rho = \rho_0(t_0/t)^3/[1 + (v/v_0)^{7.6}]$, where ρ_0 and v_0 are defined by the ejecta parameters (M and E).

We find that the steady wind $\rho \propto r^{-2}$ with density parameter $w = \dot{M}/u = 2 \times 10^{14} \text{ g cm}^{-1}$ matches the boundary velocity of the unshocked ejecta, but does not fit the CDS velocity. The appropriate model (Fig. 5) suggests an enhanced wind density at radii $r < 1.5 \times 10^{15} \text{ cm}$ and a

Table 3 Hydrodynamic models of type-IIP supernovae

SN	R_0 (R_{\odot})	M_{ej} (M_{\odot})	E (10^{51} erg)	M_{Ni} (M_{\odot})	v_{Ni}^{max} (km s^{-1})	S/A
1987A	35	18	1.5	0.0765	3000	A
1999em	500	19	1.3	0.036	660	A
2000cb	35	22.3	4.4	0.083	8400	A
2003Z	230	14	0.245	0.0063	535	S
2004et	1500	22.9	2.3	0.068	1000	S
2005cs	600	15.9	0.41	0.0082	610	S
2008in	570	13.6	0.505	0.015	770	S
2009kf	2000	28.1	21.5	0.40	7700	–
2012A	715	13.1	0.525	0.0116	710	S
2013ej	1500	26.1	1.4	0.039	6500	A
2016X	436	28.0	1.73	0.0295	4000	A
2017gmr	525	22.0	10.2	0.110	3300	A
2018gj	775	23.4	1.84	0.031	5280	A
2020jfo	400	6.2	0.756	0.013	1600	S

The last column indicates a degree of asymmetry in the ^{56}Ni ejecta. the “S” symbol stands for seemingly symmetric distribution and the “A” symbol denotes an apparent asymmetry. SN 2009kf has no clear signature for the ^{56}Ni geometry.

steady wind at $r > 1.5 \times 10^{15} \text{ cm}$ with the density parameter $w = \dot{M}/u = 8.7 \times 10^{13} \text{ g cm}^{-1}$. This wind corresponds to the mass-loss rate $\dot{M} = 2 \times 10^{-6} u_{15} M_{\odot} \text{ yr}^{-1}$ assuming the wind speed $u_{15} = u/15 \text{ km s}^{-1} = 1$.

The combined luminosity of the forward and reverse shocks at the maximum is $\approx 2 \times 10^{41} \text{ erg s}^{-1}$, lower by two orders than the maximal bolometric luminosity; a similar difference remains at later epochs. The luminosity related to the CS interaction in SN 2018gj thus is negligibly small. This conclusion is in line with the low mass of the CS shell ($3 \times 10^{-4} M_{\odot}$) within the radius $r < 1.5 \times 10^{15} \text{ cm}$, lower by almost three orders than the amount required to maintain the initial luminosity peak of SN 2018gj due to the CS interaction.

5 Discussion

The massive ejecta — the major outcome of the hydrodynamic modeling of SN 2018gj — *prima facie* seems odd, given the short plateau that presumably should be associated with a low-mass ejecta. Particularly impressive is the comparison with SN 2020jfo, another short-plateau SN IIP with the ejecta mass of $\sim 6 M_{\odot}$ (Teja et al., 2022; Utrobin and Chugai, 2024). The point, however, is that the plateau duration depends not only on the

ejecta mass, but also on the explosion energy, the pre-SN radius, the amount of ^{56}Ni , and its velocity. The inferred SN 2018gj parameters are fixed by the whole set of the relevant observables (the bolometric light curve and expansion velocities).

It should be emphasized that the crucial observables include — apart from the light curve and the photospheric velocities — the maximal velocity of the ejecta usually ignored in the hydrodynamic description of SN IIP. It is noteworthy that we recover the velocities of the external ejecta from the blue absorption wing of hydrogen lines, so these velocities somewhat exceed the velocity at the photosphere.

An interesting byproduct of the spectral analysis is the demonstration that the structure of the external high-velocity ejecta of SN 2018gj and SN 2020jfo is essentially clumpy. The clumpiness of the outer ejecta seems to be a common feature of the ordinary SNe IIP, since the clumpy structure of the external ejecta has been also recovered in type-IIP SN 2008in (Chugai and Utrobin, 2014) and SN 2012A (Utrobin and Chugai, 2015). Such a structure of the outer ejecta of SNe IIP suggests that the shock propagation during the SBO is accompanied with the fragmentation of the outer ejecta that is possibly related to the seed inhomogeneities generated by a vigorous convection in the RSG envelope. It is remarkable that the early spectra of the peculiar type-IIP SN 1987A do not reveal the $\text{H}\alpha/\text{H}\beta$ problem (Utrobin and Chugai, 2013) which is consistent with the absence of the vigorous convection in the envelope of the blue supergiant, the progenitor of SN 1987A.

The early-time boundary velocity of the ejecta combined with the $\text{H}\alpha$ HVNA permits us to recover the CS wind density that turns out to be typical for the RSG with a moderate mass-loss rate. The important implication of the found CS density is that the CS interaction luminosity is significantly lower compared to the initial bolometric luminosity of SN 2018gj. It thus rules out a notable contribution of the CS interaction to the luminosity primarily related to the radiative cooling of the exploded RSG with the radius of $775 R_{\odot}$.

The recovered ejecta mass together with the mass of the collapsing core of $1.6 M_{\odot}$ suggests the pre-SN mass of $25 M_{\odot}$. The inferred pre-SN

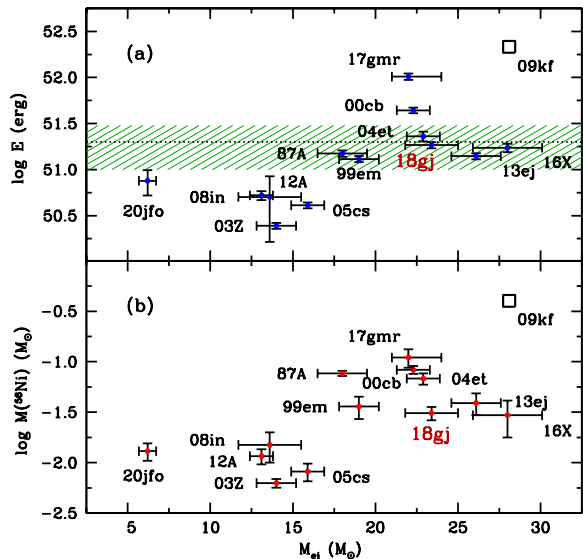


Fig. 6 Explosion energy (Panel (a)) and ^{56}Ni mass (Panel (b)) versus ejecta mass for SN 2018gj and 13 other core-collapse SNe studied using the uniform approach (Utrobin and Chugai, 2024). The dotted line in Panel (a) is the upper limit of the explosion energy of 2×10^{51} erg for the neutrino-driven mechanism (Janka, 2017) with the uncertainty of about $\pm 10^{51}$ erg² shown by the shaded green band.

mass-loss rate $\dot{M} = 2 \times 10^{-6} u_{15} M_{\odot} \text{ yr}^{-1}$ is consistent with the data for eight $25 M_{\odot}$ RSG showing \dot{M} in the range of $(0.2 - 5.6) \times 10^{-6} M_{\odot} \text{ yr}^{-1}$ (Beasor et al., 2020). The found mass-loss rate implies that the progenitor lost $\sim 1.5 M_{\odot}$ at the RSG stage. With the mass of $\sim 3 M_{\odot}$ lost earlier via a high-velocity wind at the hydrogen-burning stage (Beasor et al., 2020) one expects that the SN 2018gj initial mass on the main sequence was about $29 M_{\odot}$.

The number of SNe IIP explored via a unified hydrodynamic modeling now amounts to 14 (Table 3). Their properties are illustrated on the scatter diagrams: the explosion energy vs. the ejecta mass and the ^{56}Ni mass vs. the ejecta mass (Fig. 6). SN 2018gj does not deviate from the general behavior of the explosion energy and the ^{56}Ni mass versus the ejecta mass.

A remarkable feature of SN 2018gj is the high velocity of the ^{56}Ni ejecta. We interpret the significant blueshift of the $\text{H}\alpha$ emission at the nebular epochs (Teja et al., 2023) as an effect of the aspherical ^{56}Ni ejecta, being possibly of a bipolar geometry, likewise in SN 2004dj (Chugai et al.,

²H.-Th. Janka, private communication.

2005). Our sample of SNe IIP (Table 3) includes the events with an apparent ^{56}Ni asymmetry (7 cases) and with the seemingly symmetrical ^{56}Ni ejecta (6 events). We deliberately exclude SN 2009kf from the latter sample, because this object has the extremely high explosion energy $\approx 2 \times 10^{52}$ ergs that indicates a hypernova explosion mechanism rather than the neutrino-driven explosion of SNe IIP with the energy of $\lesssim 2 \times 10^{51}$ erg (Janka, 2017).

It is remarkable that SNe IIP with the symmetric ^{56}Ni in our sample have predominantly lower velocities of the ^{56}Ni ejecta compared to SNe IIP with the apparent asymmetry. Indeed, the mean of the ^{56}Ni outer velocity for six symmetric SNe IIP is 890 ± 340 (s.d.) km s^{-1} , whereas for seven asymmetric SNe IIP the mean is 4440 ± 2340 km s^{-1} . It should be noted that in the case of the low ^{56}Ni velocity its asymmetry is difficult to detect. The case of SN 1999em with the low ^{56}Ni velocity and the apparent bipolar $\text{H}\alpha$ asymmetry (Chugai, 2007) is an exception, possibly due to the ^{56}Ni bipolar axis being colinear with the line of sight. One can assume, therefore, that the aspherical ^{56}Ni ejecta is an intrinsic feature of all SNe IIP.

6 Conclusions

We conclude with a summary of major results:

- The hydrodynamic modeling of type-IIP SN 2018gj with the short plateau suggests the explosion of a $\approx 25 M_{\odot}$ RSG star with a radius of $\approx 775 R_{\odot}$ that ejects $\approx 23.4 M_{\odot}$ with the energy of $\approx 1.8 \times 10^{51}$ erg.
- The analysis of hydrogen lines in the early spectra reveals two major facts: (i) a high velocity of the outer ejecta ($15\,000 \text{ km s}^{-1}$) that is inconsistent with the presence of a confined massive CS shell; (ii) a clumpy structure of the outer ejecta of SN 2018gj and SN 2020jfo.
- The recovered wind density rules out a noticeable contribution of the CS interaction to the bolometric luminosity.
- The significant early escape of gamma-quanta suggests a high velocity ($\approx 5200 \text{ km s}^{-1}$) of the ^{56}Ni ejecta.
- The analysis of the sample of 13 SNe IIP studied hydrodynamically in a uniform way implies that the asymmetry of the ^{56}Ni ejecta may be an intrinsic feature of all SNe IIP.

Acknowledgements. Not applicable.

Author contribution. V.U. and N.C. contributed equally to this work.

Funding. Not applicable.

Data availability. No datasets were generated or analyzed during the current study.

Materials availability. Not applicable.

Code availability. Not applicable.

Declarations

Ethics approval and consent to participate

Not applicable.

Consent for publication

Not applicable.

Competing interests

The authors declare no competing interests.

References

- Beasor, E.R., Davies, B., Smith, N., van Loon, J.T., Gehrz, R.D., Figer, D.F.: A new mass-loss rate prescription for red supergiants. *Mon. Not. R. Astron. Soc.* **492**(4), 5994–6006 (2020) <https://doi.org/10.1093/mnras/staa255> [arXiv:2001.07222](https://arxiv.org/abs/2001.07222) [astro-ph.SR]
- Chugai, N.N., Chevalier, R.A., Utrobin, V.P.: Optical Signatures of Circumstellar Interaction in Type IIP Supernovae. *Astrophys. J.* **662**(2), 1136–1147 (2007) <https://doi.org/10.1086/518160> [arXiv:astro-ph/0703468](https://arxiv.org/abs/astro-ph/0703468) [astro-ph]
- Chugai, N.N., Fabrika, S.N., Sholukhova, O.N., Goranskij, V.P., Abolmasov, P.K., Vlasyuk, V.V.: Optical Observations of Type-IIP Supernova 2004dj: Evidence for Asymmetry of the ^{56}Ni Ejecta. *Astronomy Letters* **31**(12), 792–805 (2005) <https://doi.org/10.1134/1.2138766> [arXiv:astro-ph/0507689](https://arxiv.org/abs/astro-ph/0507689) [astro-ph]

- Chevalier, R.A.: Hydrodynamic Models of Supernova Explosions. *Fundamentals of Cosmic Physics* **7**, 1–58 (1981)
- Chevalier, R.A.: The radio and X-ray emission from type II supernovae. *Astrophys. J.* **259**, 302–310 (1982) <https://doi.org/10.1086/160167>
- Chugai, N.N.: Asymmetry of Type IIP Supernovae. In: Immler, S., Weiler, K., McCray, R. (eds.) *Supernova 1987A: 20 Years After: Supernovae and Gamma-Ray Bursters*. American Institute of Physics Conference Series, vol. 937, pp. 357–364 (2007). <https://doi.org/10.1063/1.3682929>
- Chugai, N.N.: Type IIn SN 2010jl: probing dusty line-emitting shell. *Mon. Not. R. Astron. Soc.* **481**(3), 3643–3650 (2018) <https://doi.org/10.1093/mnras/sty2386> [arXiv:1809.02478](https://arxiv.org/abs/1809.02478) [astro-ph.HE]
- Chugai, N.N., Utrobin, V.P.: Disparity between $H\alpha$ and $H\beta$ in SN 2008in: Inhomogeneous external layers of type IIP supernovae? *Astronomy Letters* **40**(2-3), 111–119 (2014) <https://doi.org/10.1134/S1063773714010010> [arXiv:1309.7814](https://arxiv.org/abs/1309.7814) [astro-ph.HE]
- Goldberg, J.A., Bildsten, L.: The Value of Progenitor Radius Measurements for Explosion Modeling of Type II-Plateau Supernovae. *Astrophys. J. Lett.* **895**(2), 45 (2020) <https://doi.org/10.3847/2041-8213/ab9300> [arXiv:2005.07290](https://arxiv.org/abs/2005.07290) [astro-ph.SR]
- Grassberg, E.K., Imshennik, V.S., Nadyozhin, D.K.: On the Theory of the Light Curves of Supernovae. *Astrophys. Space Sci.* **10**, 28–51 (1971) <https://doi.org/10.1007/BF00654604>
- Goldberg, J.A., Jiang, Y.-F., Bildsten, L.: Numerical Simulations of Convective Three-dimensional Red Supergiant Envelopes. *Astrophys. J.* **929**(2), 156 (2022) <https://doi.org/10.3847/1538-4357/ac5ab3> [arXiv:2110.03261](https://arxiv.org/abs/2110.03261) [astro-ph.SR]
- Goldberg, J.A., Jiang, Y.-F., Bildsten, L.: Shock Breakout in Three-dimensional Red Supergiant Envelopes. *Astrophys. J.* **933**(2), 164 (2022) <https://doi.org/10.3847/1538-4357/ac75e3> [arXiv:2206.04134](https://arxiv.org/abs/2206.04134) [astro-ph.SR]
- Hiramatsu, D., Howell, D.A., Moriya, T.J., Goldberg, J.A., Hosseinzadeh, G., Arcavi, I., Anderson, J.P., Gutiérrez, C.P., Burke, J., McCully, C., Valenti, S., Galbany, L., Fang, Q., Maeda, K., Folatelli, G., Hsiao, E.Y., Morrell, N.I., Phillips, M.M., Stritzinger, M.D., Suntzeff, N.B., Gromadzki, M., Maguire, K., Müller-Bravo, T.E., Young, D.R.: Luminous Type II Short-Plateau Supernovae 2006Y, 2006ai, and 2016egz: A Transitional Class from Stripped Massive Red Supergiants. *Astrophys. J.* **913**(1), 55 (2021) <https://doi.org/10.3847/1538-4357/abf6d6> [arXiv:2010.15566](https://arxiv.org/abs/2010.15566) [astro-ph.HE]
- Janka, H.-T.: In: Alsabti, A.W., Murdin, P. (eds.) *Neutrino-Driven Explosions*, p. 1095 (2017). https://doi.org/10.1007/978-3-319-21846-5_109
- Sobolev, V.V.: *Light Scattering in Planetary Atmospheres*, p. 263. Pergamon Press, Oxford, New York (1975)
- Teja, R.S., Singh, A., Sahu, D.K., Anupama, G.C., Kumar, B., A. J., N.: SN 2020jfo: A Short-plateau Type II Supernova from a Low-mass Progenitor. *Astrophys. J.* **930**(1), 34 (2022) <https://doi.org/10.3847/1538-4357/ac610b> [arXiv:2202.09412](https://arxiv.org/abs/2202.09412) [astro-ph.HE]
- Teja, R.S., Singh, A., Sahu, D.K., Anupama, G.C., Kumar, B., Nakaoka, T., Kawabata, K.S., Yamanaka, M., Takey, A., Kawabata, M.: SN 2018gj: A Short Plateau Type II Supernova with Persistent Blueshifted $H\alpha$ Emission. *Astrophys. J.* **954**(2), 155 (2023) <https://doi.org/10.3847/1538-4357/acdf5e> [arXiv:2306.10136](https://arxiv.org/abs/2306.10136) [astro-ph.HE]
- Utrobin, V.P., Chugai, N.N.: Type IIP supernova 2008in: the explosion of a normal red supergiant. *Astron. Astrophys.* **555**, 145 (2013) <https://doi.org/10.1051/0004-6361/201321678> [arXiv:1306.5122](https://arxiv.org/abs/1306.5122) [astro-ph.SR]
- Utrobin, V.P., Chugai, N.N.: Parameters of type IIP SN 2012A and clumpiness effects. *Astron. Astrophys.* **575**, 100 (2015) <https://doi.org/>

10.1051/0004-6361/201424822 arXiv:1411.6480
[astro-ph.SR]

2018-53, 1 (2018)

Utrobin, V.P., Chugai, N.N.: Resolving the puzzle of type IIP SN 2016X. *Mon. Not. R. Astron. Soc.* **490**(2), 2042–2049 (2019) <https://doi.org/10.1093/mnras/stz2716> arXiv:1909.13138 [astro-ph.HE]

Utrobin, V.P., Chugai, N.N.: Uncommon SN 2020jfo: ordinary explosion of 8 M_{\odot} red supergiant with dense wind. *Mon. Not. R. Astron. Soc.* **527**(3), 6227–6232 (2024) <https://doi.org/10.1093/mnras/stad3633> arXiv:2311.13696 [astro-ph.HE]

Utrobin, V.P., Chugai, N.N., Andrews, J.E., Smith, N., Jencson, J., Howell, D.A., Burke, J., Hiramatsu, D., McCully, C., Bostroem, K.A.: Enormous explosion energy of Type IIP SN 2017gmr with bipolar ^{56}Ni ejecta. *Mon. Not. R. Astron. Soc.* **505**(1), 116–125 (2021) <https://doi.org/10.1093/mnras/stab1369> arXiv:2105.04606 [astro-ph.HE]

Utrobin, V.P.: The Light Curve of Supernova 1987A: The Structure of the Presupernova and Radioactive Nickel Mixing. *Astronomy Letters* **30**, 293–308 (2004) <https://doi.org/10.1134/1.1738152> arXiv:astro-ph/0406410

Utrobin, V.P.: An optimal hydrodynamic model for the normal type IIP supernova 1999em. *Astron. Astrophys.* **461**, 233–251 (2007) <https://doi.org/10.1051/0004-6361:20066078> arXiv:astro-ph/0609642

Utrobin, V.P., Wongwathanarat, A., Janka, H.-T., Müller, E.: Light-curve Analysis of Ordinary Type IIP Supernovae Based on Neutrino-driven Explosion Simulations in Three Dimensions. *Astrophys. J.* **846**, 37 (2017) <https://doi.org/10.3847/1538-4357/aa8594> arXiv:1704.03800 [astro-ph.SR]

Woosley, S.E., Heger, A., Weaver, T.A.: The evolution and explosion of massive stars. *Reviews of Modern Physics* **74**(4), 1015–1071 (2002) <https://doi.org/10.1103/RevModPhys.74.1015>

Wiggins, P.: Transient Discovery Report for 2018-01-14. Transient Name Server Discovery Report